$$BW_{3dB} = \frac{1}{2\pi(R_i + R_s)C} \qquad (4.5)$$

where the R_i is 50 for RF source, the calculated bandwidth is about 12.5GHz. This can explain why we cannot achieve 40Gb/s wavelength conversion by our sample. The limit of RC constant can also be seen from Fig.4.10.

Part I of the falling tail is due to the resolution of the digital sampling oscilloscope[*] and the slow falling of part II is caused by the RC limitation. For the purpose of higher speed operation, the RC constant must be shortened. One approach to achieve this is to reduce the device capacitance by optimizing the fabrication process, or maybe more effective and simple, reducing the device length. However, as the tradeoff between the bandwidth and extinction ratio always occurs while reducing the length of a discrete external electroabsorption modulator, tradeoff between the speed and extinction ratio of our wavelength converter also inevitable. Another approach is to use chip carriers so as to spread the bandwidth and improve the response time.

4.5.3. Input power reduction

In the above experiments of wavelength conversion, the input power is still very high. How to reduce the input power? We will figure out this question in this subsection.

As mentioned, the scheme of the operation is based on the phase change difference between TE and TM, which can be calculated by the following formula,

$$\theta = \Delta\phi^{TE} - \Delta\phi^{TM} = (\Delta n^{TE}\Gamma^{TE} - \Delta n^{TM}\Gamma^{TM})L \qquad (4.6)$$

where the Δn^{TE} and Δn^{TM} stand for the change of the refractive index of TE and TM respectively, Γ^{TE} and Γ^{TM} refer to the confinement factors for TE and TM, and L is the length of the device. In our device, both Δn^{TE} and Δn^{TM} are dependent on the input power. If Δn^{TE} can be enhanced and Δn^{TM} can be reduced, then the total required power can be reduced. This can be realized by using narrower quantum well width with compressive strain.

Fig.4.13 shows the variation of quantum levels due to strain. As shown in Fig. 4.12 (b), the HH

---

[*] Because the sweep-out time of the carriers is shorter than the resolution of the digital sampling oscilloscope, the part I of the falling tall is actually due to the combination of the slow oscilloscope response and fast sweep-out time

and LH subbands degenerate at the top of valence band in lattice-matched bulk crystal and, as a result, the different quantum levels due to the difference of the effective masses of HH and LH are formed in QW. However, in tensile strained material system, on the other hand, HH goes higher than LH in bulk and the distance between the quantum levels for HH and LH become larger, as shown in Fig. 4.12 (a). Therefore, the absorption edge wavelengths for TE and TM polarizations can be made larger at zero electric field. If the absorption peak for TE mode is fixed at the specific wavelength (in EAM case, the peak wavelength is always 1490nm), then the compressive strain will shift the absorption peak to shorter wavelength compared to the lattice-matched ones.

We used the Luttinger-kohn model and finite difference method to calculate the excitonic absorption in InGaAlAs MQWs. The simulated MQWs are composed of 10-period $In_{(1-x-y)}Ga_xAl_yAs$ wells with 5nm-thick $In_{0.527}Ga_{0.206}Al_{0.267}As$ barriers. The InGaAlAs barrier layers are lattice-matched to InP substrate and the bandgap wavelength is 1100nm. We used three InGaAlAs wells for the calculations. We changed the InGaAlAs well thickness and the amount of compressive strain as 9nm with lattice-matched, 7.3nm with +0.2nm, and 6nm with +0.57%. We kept the exciton absorption wavelength for the 1st electron subband to the 1st heavy hole subband (E1/HH1) transition, which is responsible for TE mode absorption, at 1490 nm in the all three InGaAlAs MQWs above.

Fig.4.14 shows the calculated absorption coefficient spectra for InGaAlAs MQWs. Here, the external reverse bias voltages are zero. The wavelength detuning between the fundamental TE and TM mode absorption wavelengths increases with increasing the amount of the compressive strain in InGaAlAs wells and decreasing the well width. At the same time, the cross-phase-modulation (XPM) for TM mode becomes smaller at λ= 1540nm. Also, the absorption peak depths for TE mode absorptions become higher due to deeper confinement of the e1/hh1 excitons in the narrower InGaAlAs wells. In XPM, larger excitonic absorption depth in the narrower InGaAlAs wells enhances the absorption changes under the pump light, thus bringing larger phase shift for TE mode.

Fig.4.15 shows the calculated phase shifts in XPM of the EAMs with InGaAlAs MQWs mentioned above. The phase shift for TE mode become significantly larger, while that for TM mode remains small, with increasing the amount of the compressive strain and decreasing the InGaAlAs well width. The calculated phase shift for the lattice-matched InGaAlAs MQW explains well the measured TE mode phase shift, especially in high signal power region, denoted by red line. The phase shift ($\Delta\phi$) of 180-degree for TE mode is achieved at signal power

of 10dBm, 7dBm, 2dBm for the 9nm-thick lattice-matched MQW, the 7.3nm-thick +0.2% compressively strained MQW and the 6nm-thick +0.57% compressively strained MQW respectively, whereas the phase shift for TM mode are very small for all the three MQWs.

Fig.4.16 shows the phase shift differences between TE and TM mode based on the calculated results of Fig.4.15. 90-degree polarization rotation can be achieved at 13dBm, 8dBm and 3dBm for these three InGaAlAs MQW-EAMs. It is clearly shown here that the increase of the amount of the compressive strain and the decrease of the InGaAlAs well thickness enhance the polarization rotation considerably. These effects help to decrease the input power for the polarization switches and wavelength converters based on the nonlinear polarization rotation.
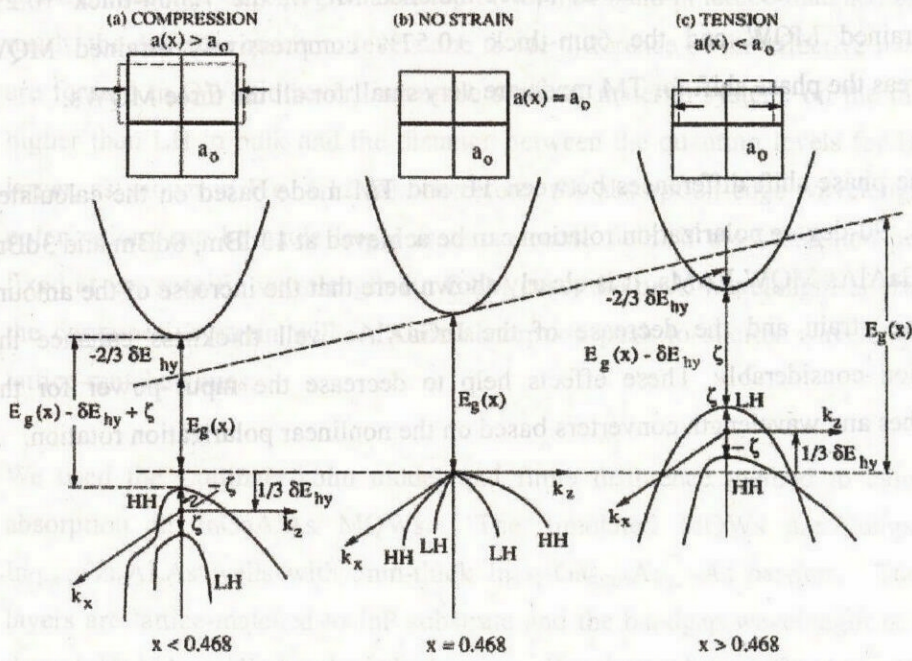
Fig. 5.13 Variation of quantum levels due to strain. (a) Compressive-strained system. (b) Lattice-matched material system. (c) Tensile-strained system.
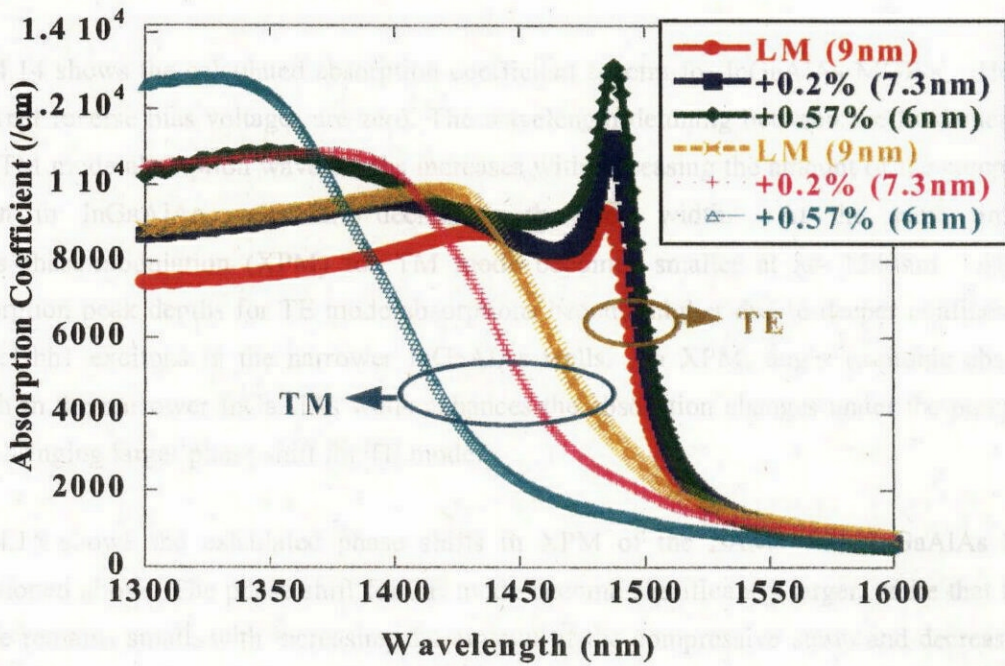

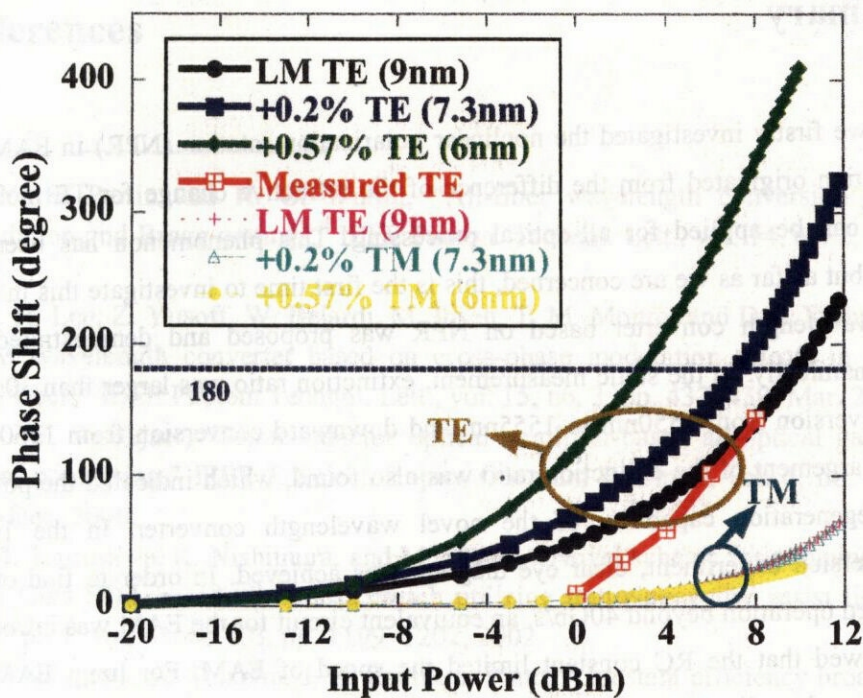Fig.4.14 Absorption coefficient spectra for the three InGaAlAs MQWs. LM denotes the lattice-matched.

Fig.4.15 The calculated phase shift for TE and TM mode by XPM in EAMs with InGaAlAs MQWs with different compressive strains and well thickness.
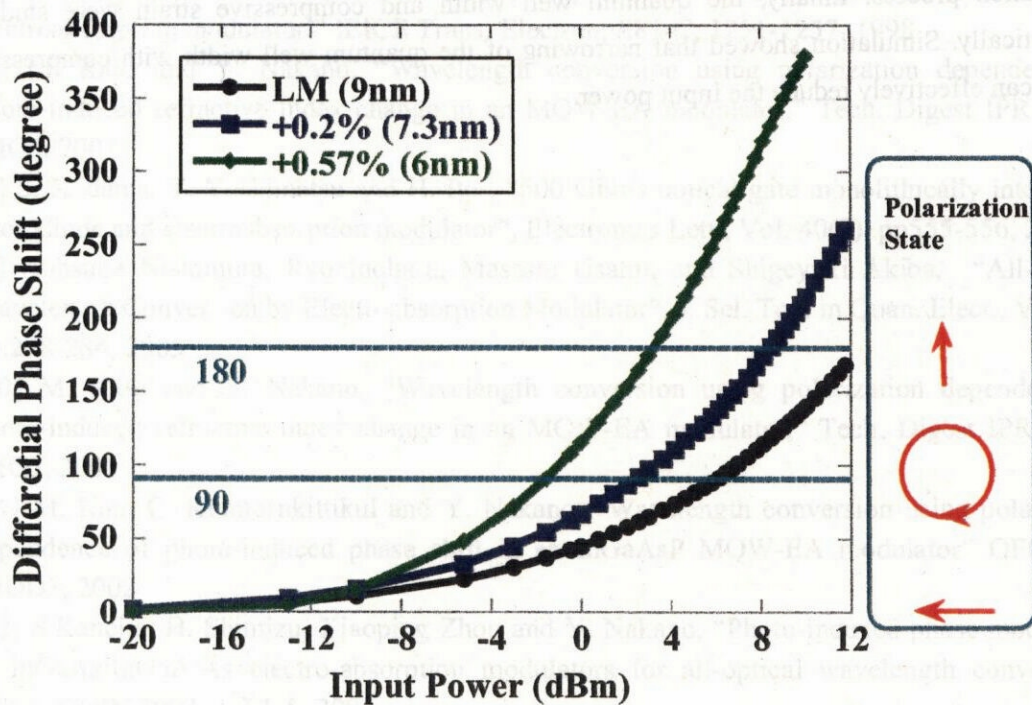

Fig.4.16 The calculated phase shift difference between TE and TM mode based on Fig. 4.15

4.6   Summary

In this chapter, we firstly investigated the nonlinear polarization rotation (NPR) in EAM. The polarization rotation originated from the difference of the refractive change for TE mode and TM mode, and can be applied for all-optical processing. This phenomenon has been well studied in SOA, but as far as we are concerned, this is the first time to investigate this in EAM. Then a novel wavelength converter based on NPR was proposed and demonstrated both statically and dynamically. In the static measurement, extinction ratio was larger than 30dB for both upward conversion from 1550nm to 1555nm and downward conversion from 1560nm to 1555nm. The enlargement of the extinction ratio was also found, which indicated the potential optical signal regeneration capability of the novel wavelength converter. In the 10Gb/s wavelength conversion experiment, clear eye diagram was achieved. In order to find out the way for high-speed operation beyond 40Gb/s, an equivalent circuit for the EAM was introduced. The analysis showed that the RC constant limited the speed of EAM. For lump EAM, the doping conditions and quality of ohmic contact of the electrode had important influence on the series resistance. Higher speed operation could be achieved by optimizing the electrode size and fabrication process. Finally, the quantum well width and compressive strain were studied theoretically. Simulation showed that narrowing of the quantum well width with compressive strain can effectively reduce the input power.

References

[1] V. E. Perlin and H. G. Winful, "All-fiber wavelength conversion using cross-phase modulation and Bragg gratings," IEEE Photon. Technol. Lett., vol. 14, no. 2, pp. 176–178, Feb. 2002.

[2] J. H. Lee, Z. Yusoff, W. Belardi, M. Ibsen, T. M. Monro, and D. J. Richardson, "A tunable WDM wavelength converter based on cross-phase modulation effects in normal dispersion holey fiber," IEEE Photon. Technol. Lett., vol. 15, no. 3, pp. 437–439, Mar. 2003.

[3] K. E. Stubkjaer, "Semiconductor optical amplifier-based all-optical gates for high-speed optical processing," IEEE J. Select. Topics Quantum Electron., vol. 6, no. 6, pp. 1428–1435, Nov./Dec. 2000.

[4] M. Tsurusawa, K. Nishimura, and M. Usami, "Novel scheme for reducing the pattern effect in 40 Gb/s SOA based all-optical switch utilizing transparent CW assist light," Jpn. J. Appl. Phys., pt. 1, vol. 41, no. 2B, pp. 1199–1202, 2002.

[5] R: Nogueira, A. Teixeira, J. da Rocha, J. Pinto, "Constant efficiency broadband wavelength converter based on self-generated orthogonal pumps", Electronics Letters,13th May 2004 Vol. 40 No. 10, pp. 616 - 617

[6] N. Edagawa, M. Suzuki, and S. Yamamoto, "Novel wavelength converter using an electroabsorption modulator," IEICE Trans. Electron, E81-C, 1251-1257, 1998

[7] M. Kato and Y. Nakano, "Wavelength conversion using polarization dependence of photo-induced refractive index change in an MQW-EA modulator," Tech. Digest IPR '2001, IMG5, 2001

[8] S. Kodama, T. Yoshimatsu and H. Ito , "500 Gbit/s optical gate monolithically integrating photodiode and electroabsorption modulator", Electronics Lett., Vol. 40(9), pp555-556, 2004

[9] Kohsuke Nishimura, Ryo Inohara, Masashi Usami, and Shigeyuki Akiba, "All-Optical Wavelength Conversion by Electroabsorption Modulator", J. Sel. Top. in Quan. Elect., V. 11(1), pp.278-284, 2005

[10] M. Kato and Y. Nakano, "Wavelength conversion using polarization dependence of photo-induced refractive index change in an MQW-EA modulator," Tech. Digest IPR '2001, IMG5, 2001

[11] M. Kato C. Kumtornkittikul and Y. Nakano, "Wavelength conversion using polarization dependence of photo-induced phase shift in an InGaAsP MQW-EA modulator" OFC'2002, ThDD3, 2002

[12] S.Kaneko, H. Shimizu, Xiaoping Zhou and Y. Nakano, "Photo-induced phase modulation in InGaAs/InGaAlAs electro-absorption modulators for all-optical wavelength conversion", OECC/COIN 2004, 14F1-5, 2004

[13] M. Kato and Y. Nakano , "Wavelength and material dependence of photo-induced phase shift in multiple-quantum-well electro-absorption modulators"OECC'2001, 591-592, 2001

[14] Qiang Lin and Govind P. Agrawal, "Vector Theory of Cross-Phase Modulation: Role of Nonlinear Polarization Rotation", JOURNAL OF QUANTUM ELECTRONICS, Vol.40(7),

pp958-966, 2004

[15] H. J. S. Dorren, Daan Lenstra, Yong Liu, Martin T. Hill, and Giok-Djan Khoe, "Nonlinear Polarization Rotation in Semiconductor Optical Amplifiers: Theory and Application to All-Optical Flip-Flop Memories", JOURNAL OF QUANTUM ELECTRONICS, Vol.39(1), pp.141-148, 2003

[16] Y. Liu, M. T. Hill, E. Tangdiongga, H. de Waardt, N. Calabretta, G. D. Khoe, and H. J. S. Dorren, "Wavelength Conversion Using Nonlinear Polarization Rotation in a Single Semiconductor Optical Amplifier", PHOTONICS TECHNOLOGY LETTERS, Vol.15(1), pp.90-92, 2003

[17] A. K. Mishra, X. Yang, D. Lenstra, G.-D. Khoe, and H. J. S. Dorren, "Wavelength Conversion Employing 120-fs Optical Pulses in an SOA-Based Nonlinear Polarization Switch", JOURNAL OF SELECTED TOPICS IN QUANTUM ELECTRONICS, Vol.10(5), pp.1180-1186, 2004

[18] H. Shen, M. Wraback, J. Pamulapati, M. Dutta, P. G. Newman, A. Ballato,and Y. Lu, "Normal incidence high contrast multiple quantum well light modulator based on polarization rotation," Applied Physics Letters, Vol.62(23), pp.2908-2910, 1993